Journal of Applied Polymer Science

# Synthesis and Characterization of Fibrous Nanosilica/Polydimethylsiloxane Composites

**Nabarun Roy,[1] Anil K. Bhowmick[1,2]**
[1]Indian Institute of Technology, Kharagpur 721302, India
[2]Department of Chemistry, Indian Institute of Technology, Patna 800013, India
Correspondence to: A. K. Bhowmick (E-mail: anilkb@rtc.iitkgp.ernet.in) or (E-mail: director@iitp.ac.in)

**ABSTRACT:** This article reports the synthesis of silica nanofiber/polydimethylsiloxane composites. Hollow silica nanofibers were synthesized through soft-template mediated synthesis using nitric acid catalyst and extensively characterized. Amorphous nanofibers were obtained by this method with mean diameter of 80 nm and length extending over several micrometers. Nanofibers were also prepared by varying the surfactant concentration and its effect on aspect ratio was investigated. Incorporation of these nanofibers into PDMS matrix was accomplished through *in situ* and *ex situ* preparative techniques. The composites prepared exhibited a significant enhancement of various properties. *In situ* prepared composites yielded maximum improvement in properties with 120% improvement in tensile strength, 175% improvement in room temperature storage modulus and 190°C increase in temperature of maximum degradation ($T_{max}$) even at low filler loading. Extent of nanofiller dispersion solely determined the property improvement of the composites. Nanofiller aspect ratio was also found to play an important role on the property improvement of the composites. Composite formation and hence property improvement were explained in depth in the light of free energy change and interaction parameter of the components of the hybrid material. © 2013 Wiley Periodicals, Inc. J. Appl. Polym. Sci. 130: 1005–1019, 2013

**KEYWORDS:** polydimethylsiloxane; silica nanofiber; composites; properties; characterization; ring-opening polymerization; rubber; nanofiber

Received 26 December 2012; accepted 25 February 2013; published online 17 April 2013
**DOI: 10.1002/app.39229**

## INTRODUCTION

Organic/inorganic nanofibers based polymer composites demonstrate a blend of elegant properties such as light weight and excellent mechanical and thermal properties. Nanofibers dispersed in a polymer matrix behave as stress transferring machineries and hence are effective in enhancing modulus and strength of the prepared composites.[1] Improvement in mechanical property in these reinforced composites is a function of the aspect ratio and orientation of the nanofibers. In fact, enhanced adhesion at the polymer-filler interface is responsible for the improved fatigue resistance, toughness and tensile properties. In the case of nanofiber reinforced composites, the reinforcing mechanism varies with temperature. When polymer is in the glassy state, nanofiber reinforcement is entirely reliant to the load transferring efficiency of nanofibers. On the other hand, in the rubbery state, hydrodynamical factor and reinforcement due to rubber-nanofiber interaction are responsible for property improvement owing to formation of rigid rubber-nanofiber network.[2]

The field of nanoscience was amalgamated with that of polymer technology by the Toyota Central R&D Laboratories in fabricating nanoclay/nylon6 composites with superior mechanical properties.[3] From then onwards, silica,[4–6] nanoclay,[7–10] and various other nanoparticles have been successfully incorporated in various polymeric systems to generate hybrid materials with a blend of properties unattainable with either of the components alone. Effect of morphology of nanofiller on mechanical reinforcement has also been investigated. Literature provides a handful of examples where superiority of nanofibers, nanotube or nanowhisker over spherical nanoparticles as a reinforcing element has been provided.[11–13]

Polydimethylsiloxane (PDMS) has unique combination of inherent low temperature flexibility and high temperature stability. In addition, its excellent biocompatibility and self healing properties have opened a new avenue in biomedical applications such as artificial implants and prosthetics etc. A recent trend in the field of nanotechnology involves designing of hybrid nanomaterials out of PDMS using CNTs,[14–17] CNFs,[18,19] graphite,[20,21] or nanoclay[22–24] and several other unconventional nanofillers such as vanadate,[25] zirconium oxo species,[26] etc. Due to similarity in chemical linkages, silica has been extensively used

in reinforcing silicone rubber.[27,28] This system has been a matter of in-depth research since incredible results in terms of property improvement was achievable by including few weight percent of nanosilica in to PDMS matrix.[29–33] The improvement was attributed to alteration in chain dynamics of the macromolecules near the interface.[30,31] Despite this comprehensive study, no work has been pursued on the effect of aspect ratio of the silica nanofiber in silicone rubber reinforcement. Literature offers a few investigations on synthesis of silica nanotubes and nanofibers using a variety of reagents and reaction conditions. As for instance, Adachi et al. provided a surfactant assisted route for silica fiber synthesis using tetraethylorthosilicate as the precursor and laurylamine hydrochloride as the catalyst.[34] In another case, Shen et al. practiced a thermal evaporation technique in preparation of silica nanotubes having varying lengths and diameters.[35] These materials are used as molecular sieves and catalyst in various reactions and as protective coatings on corrosion-prone materials. However, there is as such no report on the reinforcing behavior of these unique materials in a polymer matrix. Also the preparation technique can be microengineered to suit the applications of polymer composites. Hence, there is enough opportunity to carry out a broad understanding of the structure and property of the composites prepared with silica nanotubes or nanofibers.

In this study, we synthesized silica nanofibers through hydrolysis-condensation mechanism via a surfactant assisted template approach. Here, cetrimide was used for the first time to generate the template for silica nanofiber synthesis. Varying amounts of the surfactant were used to determine its effect on the shape of the generating nanofiber. The nanofibers were characterized by using high resolution transmission electron microscope (HRTEM), wide angle X-ray diffraction (WAXD), BET $N_2$ adsorption studies and Fourier transform-infrared (FT-IR) spectroscopy. The next phase of the study depicts the PDMS composite synthesis with silica nanofibers through *in situ* polymerization and *ex situ* solution blending techniques. The feasibility of the composite formation was ascertained thermodynamically. Mechanical, dynamic mechanical, and thermal properties were extensively investigated and correlated with the morphology of these hybrid materials. The effect of the nanofiber aspect ratio on the extent of dispersion and hence on property improvement of the composites was also examined. This kind of elaborate study with this system taking into consideration various parameters such as nanoparticle aspect ratio and its extent of dispersion and effect of calcination of nanofibers on composite property enhancement has not been carried out earlier, to the best knowledge of the authors.

## EXPERIMENTAL

### Materials

Tetraethylorthosilicate (TEOS) and nitric acid (used as catalyst) required for silica nanofiber generation were procured from Acros Organics, NJ, and Merck, India respectively. Template for nanofiber generation was synthesized using cetrimide which was acquired from Merck, India. Octamethylcyclotetrasiloxane $[(CH_3)_2SiO]_4$ ($D_4$), the cyclic precursor for polydimethylsiloxane possesses a boiling point of 175°C, viscosity of 1.396, density of 0.955 and purity >99% (GC). This was received from Momentive Performance Materials, Bangalore, India; 1,1,3,3-tetramethyl-1,3-divinyldisiloxane (purity 97%) with a boiling point of 139°C and a density of 0.809, was used to add vinyl functionality to the polymer. This material was obtained from Sigma-Aldrich. Curing agent consisted of platinum catalyst (Pt catalyst in U-10, where U-10 is a vinyl PDMS system with molecular weight 74,400 and viscosity 10 Pa s having a hydride content of 0.05 mmol/g) and the hydride crosslinker polymethylhydrogenosiloxane (V430) (chemical formula $Me_3Si(OSiMe_2)_x(OSiMeH)_yOSiMe_3$, where $x$ and $y$ are 10, having Si-H content of 4.3 mmol/g). These reagents were provided by Momentive Performance Materials, Bangalore, India. Potassium hydroxide and phosphoric acid were obtained from Merck, Mumbai, India.

### Synthesis of Silica Nanofibers

Cetrimide (surfactant) (6.3 g; 0.018 mol) of was dissolved in 100 mL of deionized water for 30 min in a 250 mL beaker using a magnetic stirrer in order to ensure a homogeneous medium. Twenty grams (0.32 mol) of concentrated nitric acid was added through a dropping funnel into the mixture subjected to continuous stirring for another 30 min. A constant temperature of 28 to 30°C was maintained throughout the whole process by a cooling arrangement. The resultant mixture was stirred for additional 20 min followed by addition of 25.3g (0.12 mol) of TEOS through a dropping funnel. This triggered a milky suspension formation followed by precipitation of the nanoparticles. Stirring was continued for 1 hr and then the solution was left undisturbed overnight to facilitate complete growth of the nanofibers. The suspension was subjected to autoclave treatment at 120°C for 4 hr. Work-up was initiated by decanting off the supernatant and thorough washing of the as-prepared nanoparticles with ethanol followed by water. The washed nanofibers were then dried in an oven at 80°C for 24 hr. These constituted the uncalcined silica nanofibers. The washed and dried nanofibers were calcined in a muffle furnace at 500°C for 8 hr.

Silica nanofibers were also prepared by varying the amounts of cetrimide. Two batches were prepared with 3.15 g (0.009 mol) and 12.6 g (0.036 mol) of cetrimide with the same reagents and identical reaction conditions. The nanofibers prepared with 0.009, 0.018, and 0.036 mol were designated as SU′, SU, and SU″, respectively.

### Preparation of Silica Nanofibers/PDMS Composites

***In Situ* Polymerization Technique.** Fifteen grams of $D_4$ and 0.08 g KOH were taken in a dry $N_2$ gas purged three-necked round-bottomed flask fitted with a condenser. Reaction was initiated in a silicone oil bath placed on a hot plate at a temperature of 140°C provided with a stirring arrangement. The reaction mixture showed a steady rise in viscosity with time. The as-prepared and calcined silica nanofiber was added into the reaction mixture after 30 min of the initiation of the reaction with a constant stirring rate of 300 rpm. This was followed by addition of the vinyl terminator at the end of 2 hr of the initiation. The polymerization reaction was terminated at the end of 4 hr which was followed by reaction workup using phosphoric acid and curing with Pt catalyst-Si-H curing system.

**Table I.** Summary of the Sample Preparation Details Along with Their Designation

| Composite | Method of preparation | Nanofiller | Filler concentration (wt %) |
|---|---|---|---|
| VPSU2(THF) | Solution mixing using THF | Uncalcined silica nanofiber SU | 2 |
| VPSU4(THF) | Solution mixing using THF | Uncalcined silica nanofiber SU | 4 |
| VPSU2(TOL) | Solution mixing using toluene | Uncalcined silica nanofiber SU | 2 |
| VPSU2I | *In situ* polymerization | Uncalcined silica nanofiber SU | 2 |
| VPSU4I | *In situ* polymerization | Uncalcined silica nanofiber SU | 4 |
| VPSU6I | *In situ* polymerization | Uncalcined silica nanofiber SU | 6 |
| VPSC2(THF) | Solution mixing using THF | Calcined silica nanofiber SC | 2 |
| VPSC2I | *In situ* polymerization | Calcined silica nanofiber SC | 2 |
| VPSC4I | *In situ* polymerization | Calcined silica nanofiber SC | 4 |
| VPSU′4I | *In situ* polymerization | Uncalcined silica nanofiber SU′ | 4 |
| VPSU″4I | *In situ* polymerization | Uncalcined silica nanofiber SU″ | 4 |

**Solution Mixing.** Thirteen grams of the synthesized polymer was dissolved in appropriate solvent to form a homogeneous solution. In a separate beaker, stoichiometric quantities of silica nanofiber were dispersed in a suitable solvent through stirring and sonication. This suspension was gradually added to the polymer solution with constant stirring. The resulting mixture was stirred and sonicated. To this mixture curing agents were added followed by casting in a teflon petridish. The transparent sheets obtained were oven-dried at 80°C. A summary of the samples prepared by various methods along with their designation is provided in Table I.

**Characterization**

Morphological analysis of the silica nanofibers was pursued through HRTEM of the powdered uncalcined and calcined samples. In order to achieve this, a small amount of the powdered sample was dispersed in deionized water by ultrasonication at 45 kHz for 1 hr. A minute amount of this mixture was dropped through a microliter syringe on a carbon coated copper grid. Microscopy was executed with JEOL 2100, Japan, which was operated at an accelerating voltage of 200 kV. Morphology of the composites was resoluted through HRTEM analysis of the samples prepared by ultramicrotomy.

Crystallinity of the nanofibers as well as the composites was investigated through WAXD analysis. Analysis was done through a Rigaku TT RAX 3 XRD machine with a Cu target, using Cu-K$\alpha$ radiation ($\lambda$ = 1.54 Å), at 2 to 40° Bragg's angle value. The operating voltage was set at 40 kV while current for the measurement was fixed at 20 mA.

FT-IR studies of the as-synthesized and calcined nanofibers were performed using Perkin Elmer FT-IR–spectrophotometer (model spectrum RX I), over a range of 400 $cm^{-1}$ to 4400 $cm^{-1}$ using a resolution of 4 $cm^{-1}$. The tests were done by preparing KBr pellets of the powdered samples. Analysis of the composites was executed through attenuated total reflection (ATR)–FT-IR spectroscopy. The tests were carried out with an infrared spectrophotometer (Nicolet Nexus, Madison, WI) within a range of 650 $cm^{-1}$ to 4000 $cm^{-1}$ taking a resolution of 4 $cm^{-1}$ using a ZnSe prism.

Surface area of the calcined nanofiller was investigated from nitrogen adsorption studies using surface area analyzer Smart Sorb 92/93 at 25°C.

In contact angle measurements, double distilled water and formamide were used as the two probe liquids for measurement. Contact angle measurement was done using Kernco, Model GII contact angle meter. The surface energy of the unfilled PDMS was calculated using the Owens and Wendt equation:

$$\cos\theta = -1 + \frac{2(\gamma_s^d\gamma_l^d)^{1/2}}{\gamma_l} + \frac{2(\gamma_s^p\gamma_l^p)^{1/2}}{\gamma_l} \quad (1)$$

where $\gamma$ is the surface energy, $d$ and $p$ are the dispersive and polar components and $s$ and $l$ are solid and liquid respectively. $\theta$ is the contact angle of measurement. The surface energy values for the two liquids were obtained from the literature.[36]

Considering the phenomenon of composite formation as wetting of the nanofiller surface by the polymer, the interfacial interaction energy is expressed as:

$$\gamma_{s's} = \gamma_{s'} + \gamma_s - 2(\gamma_{s'}^d\gamma_s^d)^{1/2} - 2(\gamma_{s'}^p\gamma_s^p)^{1/2} \quad (2)$$

where $\gamma_{s'}$ and $\gamma_s$ are the surface energies of silica nanofiller and PDMS and $d$ and $p$ are the dispersive and polar components. The value of $\gamma_{s'}$ is obtained from literature.[37]

Hence, the work of adhesion is calculated as:

$$\text{Work of adhesion } W_A = \gamma_{s'} + \gamma_s - \gamma_{s's} \quad (3)$$

The swelling study of the composite specimens was carried out in toluene at ambient conditions (27°C) for 72 hr. The volume fraction of rubber in swollen gel ($V_r$) is calculated using following equation:[38]

$$V_r = \frac{(D_s - F_f A_w)\rho_r^{-1}}{(D_s - F_f A_w)\rho_r^{-1} + A_s\rho_s^{-1}} \quad (4)$$

where $A_w$ = weight of sample; $F_f$ = weight fraction of insoluble components; $D_s$ = deswollen weight of the sample; $A_s$ = weight of absorbed solvent determined for swelling increment; $\rho_r$ = density of rubber; $\rho_s$ = density of the solvent.

The crosslink density was resoluted using the Flory-Rehner equation[39] which is as follows:

$$-[\mathrm{In}(1 - V_r) + V_r + \chi V_r^2] = \frac{\rho_r}{M_c} \times V_s\left(V_r^{1/3} - \frac{V_r}{2}\right) \quad (5)$$

where, $M_c$ = molecular weight between crosslinks; $V_s$ = molar volume of the solvent; $\chi$ = Flory–Huggins interaction parameter (its value is 0.465 for PDMS–toluene system).

The results shown were mean values of three experiments performed for each sample with a mean error of ±3% for the measurements.

Differential scanning calorimetry was carried out using Perkin-Elmer DSC 8000. The temperature range was set at −150°C to 50°C and the run was carried out at a heating rate of 10°C/min.

Dynamic mechanical analysis of the composites was performed using a DMA of TA instruments (model Q800). A constant frequency of 1 Hz, a strain of 0.05% and a temperature range from –125 to 50°C at a heating rate of 3°C/min were employed to test the properties whereby storage modulus ($E'$) and loss tangent (tan $\delta$) were measured as a function of temperature.

The tensile tests were performed with the specimens punched out from the oven-dried samples with a ASTM Die-C using a Zwick UTM, Model—Z010 (Zwick GmbH and Co., Ulm, Germany) at a cross-head speed of 500 mm/min at room temperature.

Thermal stability of the composites was measured using a Perkin Elmer TGA Instrument, Diamond TG-DTA and the data were analyzed by Perkin Elmer analysis software. Samples (around 5 mg) were heated in air atmosphere up to 800°C at a heating rate of 20°C/min. The results produced had an error of ±1°C.

## RESULTS AND DISCUSSION

### Characterization of the Nanofibers

Figure 1(a,b) shows respectively the HRTEM micrographs of the as-prepared silica nanofibers SU and the calcined SC samples. The micrographs reveal a unique morphological characteristic of the nanofibers prepared by soft template-assisted approach. By virtue of the method of preparation, the silica particles assume fiber-like morphology with an average thickness of 80 nm and length reaching several micrometers. The nanofibers are observed to possess hollow core (with a mean diameter of 50 nm), which is observed as the illuminated middle part of the fibers, surrounded by a wall of around 10 to 30 nm thickness (bamboo-like structure). High temperature treatment results in thinning of the nanofibers with decrease in the dimension or complete disappearance of the hollow core as in the case with most nanofibers. The calcined samples feature more regular and distinctly visible walls. Width of the central hollow portion and the thickness of the walls, however, vary significantly resulting in high polydispersity of the synthesized nanofibers. SAED analysis [as evident from Figure 1(c)] of the calcined nanofibers ensures complete amorphousness. WAXD analysis of both as prepared and calcined nanofiller shows a broad hump spanning a broad $2\theta$ region of 15 to 30° justifying amorphicity of the nanofiller prepared by this method. This is depicted in Figure 1(d).

BET nitrogen absorption studies were conducted in order to estimate the surface area of the calcined nanofibers. The surface area was found to be 222 $m^2/g$.

The FT-IR spectra of the synthesized nanofibers (Figure 2) ensure all the characteristic structural features of silica. Presence of bands around 1080 $cm^{-1}$ (Si-O-Si asymmetric stretching), 807 $cm^{-1}$ (Si-O-Si skeletal stretching) and 3500 $cm^{-1}$ (Si-OH stretching) guarantees nanosilica formation. The uncalcined sample shows a small doublet in the region of 2900 $cm^{-1}$. This is probably due to the presence of the surfactant molecules on the nanofiber surface. This peak is removed when the nanofibers are subjected to heat treatment. In addition, the calcined sample shows a prominent reduction in the intensity of the peak at 3500 $cm^{-1}$ compared with the uncalcined nanofiller due to removal of adsorbed water molecules as well as condensation of adjacent silanol groups.

An attempt was made to investigate the effect of cetrimide on the shape and aspect ratio of the nanofibers. It was found that with 0.009 mol of cetrimide, the nanofibers obtained possessed large aspect ratio. The nanofibers SU′ [Figure 3(a)] possessed diameter in the range of 40 to 60 nm (with the hollow core diameter of around 10 nm or even less) and extending over several micrometers even longer than one obtained for SU. On the other hand, the fibers obtained in the case of SU″ [Figure 3(b)] showed very small aspect ratio since the fibers thickened (with mean thickness of 140–160 nm) and length of about 1 to 1.5 $\mu$m. The diameter of the hollow core also increased with a mean value of 80 nm.

### Probable Mechanism of Silica Nanofiber Formation

The silica nanofibers are prepared by sol-gel reaction of tetraethylorthosilicate (TEOS) using $HNO_3$ as the catalyst. The morphology of the nanofibers was designed using a soft template assisted method. In this work, we aimed at synthesizing nanoparticles having fiber-like morphology. This was achieved through a template designed using a surfactant (cetrimide). Tuning of pH of the solution resulted in spherical to rod transition of the micelle.[40] Since water was used as the medium, the surfactant is assumed to favorably form micelle with polar heads towards the aqueous phase, while the hydrophobic tails aggregated at the centre of the micelle. TEOS molecules being soluble in water probably co-ordinate with electron deficient N atom through the lone pair electrons on the O atoms as shown in A (Figure 4). The $H^+$ ions present in the aqueous medium catalyze the hydrolysis of TEOS and hence trigger the formation of silica as shown in B. Workup of the product results in

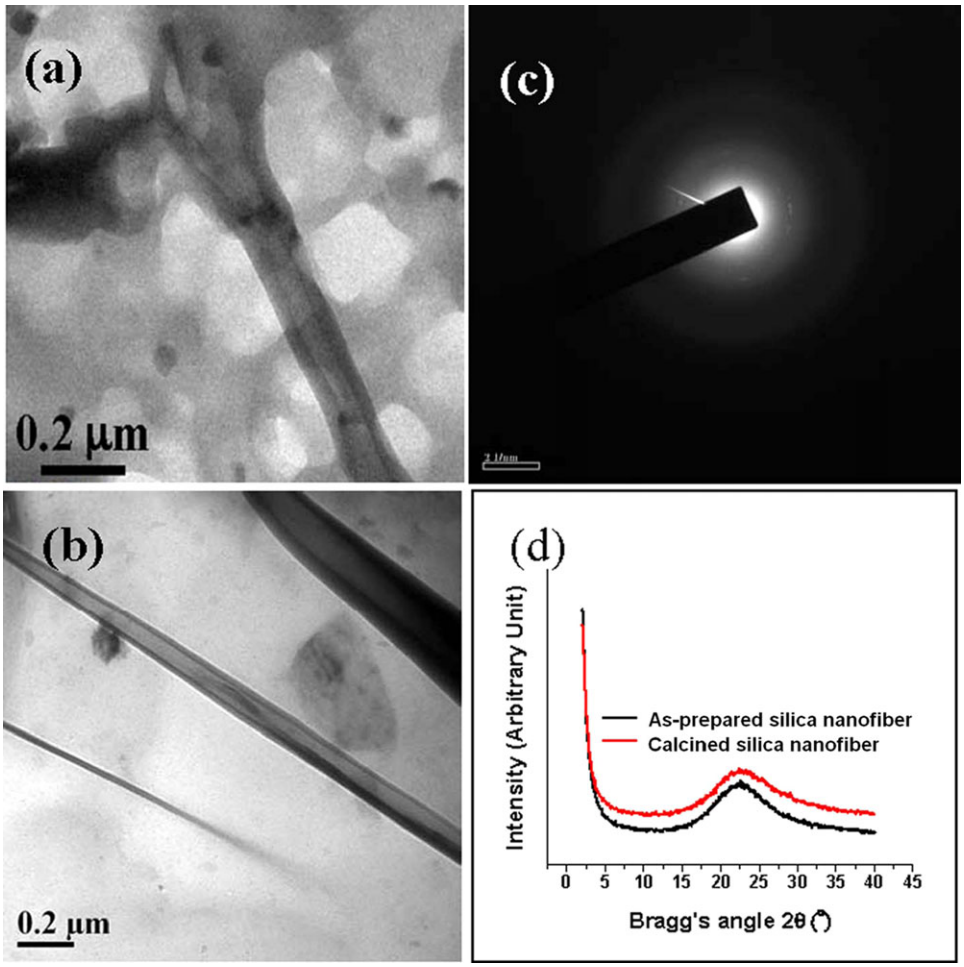


**Figure 1.** Representative HRTEM micrographs of (a) uncalcined (SU) and (b) calcined (SC) silica nanofibers; (c) SAED image of calcined silica nanofibers and (d) WAXD profiles of uncalcined and calcined nanofillers. [Color figure can be viewed in the online issue, which is available at wileyonlinelibrary.com.]

removal of the surfactants, thereby resulting in the hollow core of the nanofibers as shown in C. At low cetrimide concentration, the surfactant molecules might undergo a spherical to rod transition at an acidic pH (in presence of $HNO_3$). Hence the SU′ nanofibers are very long with high aspect ratio. With increase in surfactant concentration, there might an opposing driving force which tends to undergo a reversal even in acidic medium. Hence, nanofibers become shorter and thicker. This was observed for the nanofibers, SU″, which have lower aspect ratio. The nanofibers further undergo shortening and thickening with increased core diameter for SU″. Hence, probably there is a rod to sphere or near sphere transition in presence of excess surfactant molecules. The probable scheme of the formation of silica nanofiber is shown pictorially in Figure 4.

### Characterization of the PDMS Composites

Synthesis and characterization of vinyl terminated PDMS was reported in our previous publication.[23] In short, vinyl terminated PDMS was synthesized by anionic ring opening polymerization of octamethylcyclotetrasiloxane with potassium

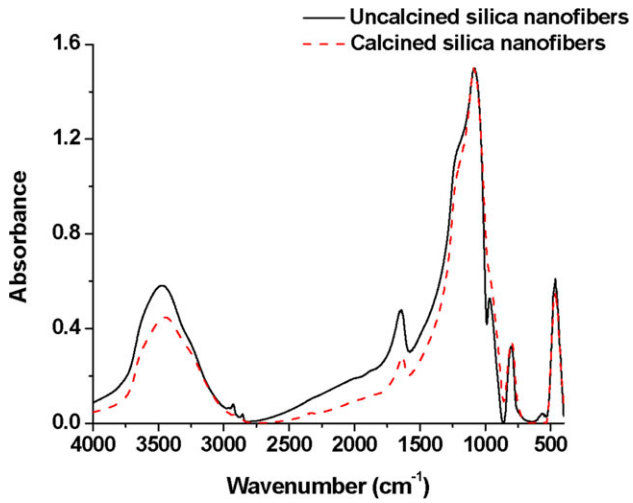


**Figure 2.** FT-IR spectra of the uncalcined and calcined silica nanofibers. [Color figure can be viewed in the online issue, which is available at wileyonlinelibrary.com.]

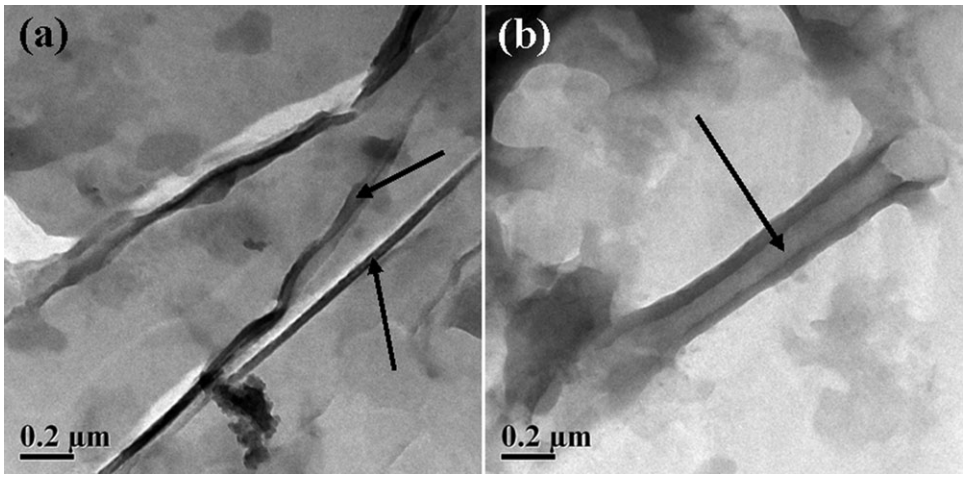


**Figure 3.** Representative HRTEM micrographs of (a) SU′ and (b) SU″.

hydroxide as the initiator. The molecular weight of the synthesized polymer was estimated to be ~91,000 which remained unchanged when polymerization was carried out in presence of nanofiller. The composites were prepared by both *in situ* and *ex situ* techniques, as described in the experimental section. This section describes characterization of these composites.

**HRTEM Analysis.** Morphology of the composites prepared by various methods was examined through HRTEM analysis. Superior dispersion was achieved when composite was prepared through *in situ* polymerization technique. This is discernible from the representative HRTEM image of the *in situ* prepared composite with 2 wt % of silica nanofiber SU (VPSU2I) [Figure 5(c)]. In this representative micrograph, individual nanofibers are found dispersed uniformly in the PDMS matrix. The best dispersion of nanofibers is probably due to the fact that polymerization takes place in presence of nanofibers in this case. This phenomenon assists better dispersion of nanofibers by debundling.

It was also observed that degree of dispersion of the nanofibers in the *ex situ* prepared composites was solely reliant upon the solvent system used during composite preparation. For VPSU2 in toluene, agglomerates of the nanofillers in the form of intertwined network were detected at various parts of the microtomed sample. A representative image is the one shown in Figure 5(a) However, for a good solvent system (THF in this case) dispersion of the nanofiller was markedly improved. This is noticed from the HRTEM image of VPSU2(THF) in Figure 5(b).

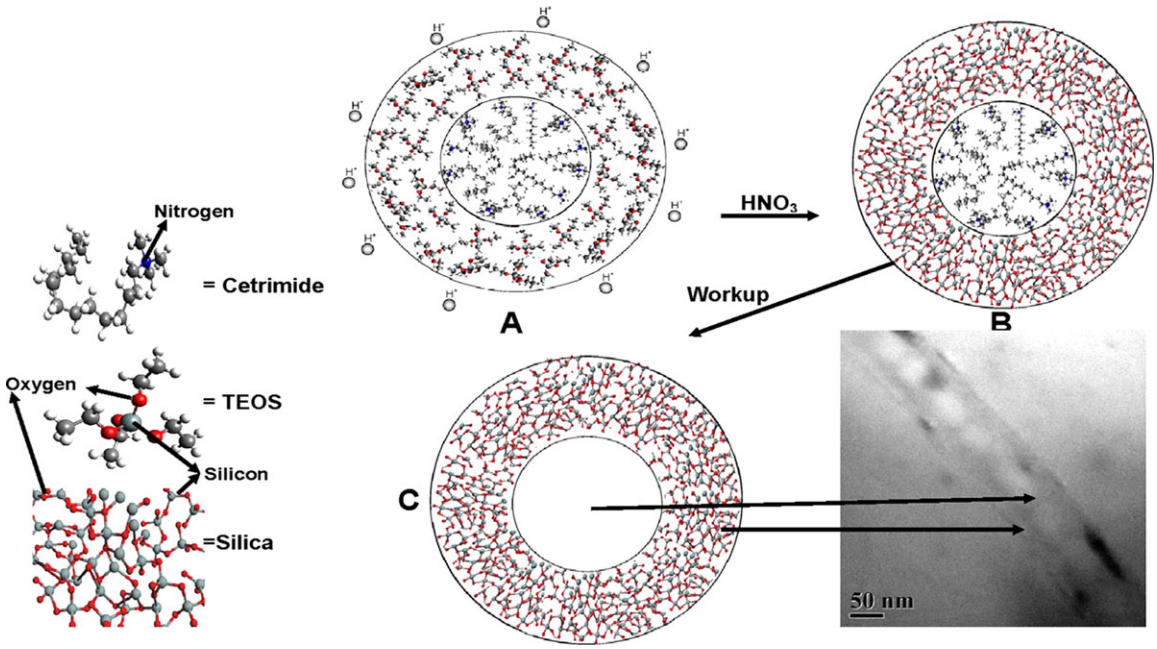


**Figure 4.** Plausible mechanism of template assisted silica nanofiber formation (cross-sectional view of the nanofiber has been shown). [Color figure can be viewed in the online issue, which is available at wileyonlinelibrary.com.]

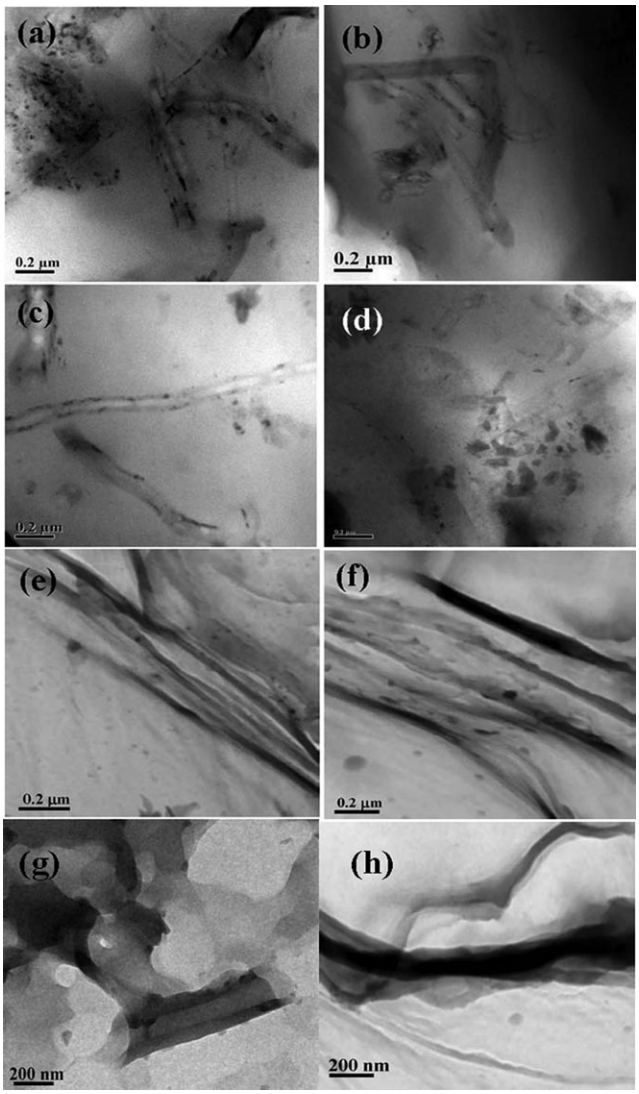


**Figure 5.** Representative HRTEM images of the composites (a) VPSU2(TOL), (b) VPSU2(THF), (c) VPSU2I, (d) VPSU4I, (e) VPSC2(THF), (f) VPSC2I, (g) VPSU″4I, and (h) VPSU′4I.

With increase in nanofiller content, composites showed few agglomerated regions along with regions of well dispersion. This is observed in the HRTEM micrograph of VPSU4I shown in Figure 5(d). With even higher loading, agglomeration was more prominent.

Composites prepared with calcined silica nanofibers SC did not essentially exhibit significant difference in the degree of dispersion when compared with those prepared with uncalcined nanofibers, as shown in Figure 5(e,f). However, the micrographs clearly speak of well-defined contours of the nanofibers upon calcination. Uncalcined nanofibers with irregular surface facilitate improved polymer-filler interaction (discussed later) through the interlocking phenomenon. However, once the surface becomes smooth with well defined contours, there is chain slippage and interlocking sites are less. This probably affects polymer-filler interaction. For the uncalcined nanofibers, the walls of the nanofibers are irregular as observed from Figure 1(a). Upon calcination, the nanofibers suffer a prominent reduction in thickness as observed from the HRTEM image in Figure 1(b). In addition, the calcined nanofibers show well defined and smooth walls. As evident from the morphological analysis of the powdered samples as well as composites, the uncalcined and calcined silica nanofibers show a mean thickness of 80 nm and 60 nm, respectively. In both the cases, some fibers with larger diameter are observed which are probably due to aggregation of smaller fibers.

Quantification of the degree of dispersion was done using the dispersion parameter $D_{0.1}$ similar to our previous publications.[18,19] The dispersion degree parameter is expressed as:

$$D_{0.1} = 1.1539 \times 10^{-2} + 7.5933 \times 10^{-2}(\bar{x}/s) + 6.6838 \times 10^{-4}(\bar{x}/s)^2 - 1.9169 \times 10^{-4}(\bar{x}/s)^3 + 3.9201 \times 10^{-6}(\bar{x}/s)^4 \quad (6)$$

where $\bar{x}$ is the mean spacing between the silica nanofibers and $s$ is the standard deviation.

For VPSU2I a $D_{0.1}$ value of 3.42% was found while VPSU2(THF) showed a lower $D_{0.1}$ value (2.77%). Hence, *in situ* prepared composites showed better nanofiller dispersion compared with the *ex situ* prepared composites at similar filler loading.

Degree of dispersion was also dependent on the aspect ratio of the nanofiber. For VPSU″4I [Figure 5(g)], the fibers being shorter are easily dispersed almost homogeneously in the polymer matrix with a $D_{0.1}$ value of 3.32%. However, in the case of the composite VPSU′4I, the nanofibers are very difficult to disperse in the PDMS matrix due to their extremely large aspect ratio. The nanofibers remain entangled as observed from the representative micrograph shown in Figure 5(h). The composite showed a $D_{0.1}$ value of 1.33%. The difference in degree of dispersion is well reflected in the properties of the composites.

**WAXD Studies.** Figure 6 exposes a comparison of the XRD profiles of the composites prepared with silica nanofibers

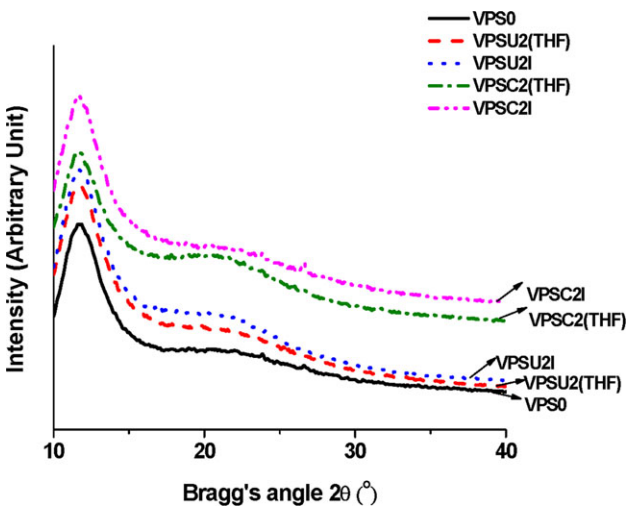


**Figure 6.** Comparison of the WAXD profiles of the unfilled and silica nanofiber filled PDMS vulcanizates. [Color figure can be viewed in the online issue, which is available at wileyonlinelibrary.com.]

Applied Polymer SCIENCE

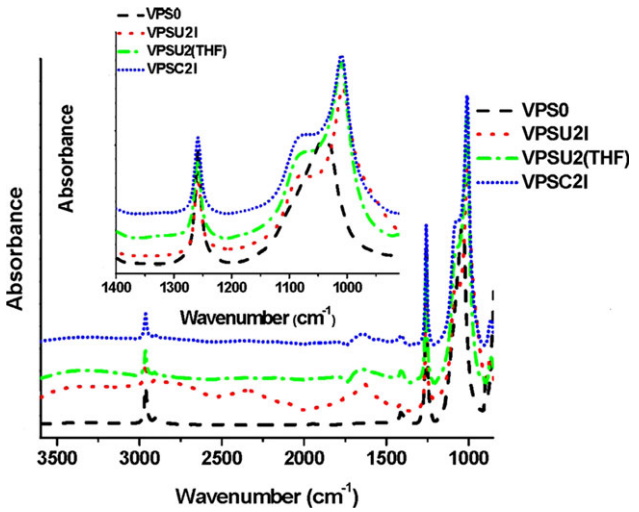


**Figure 7.** Comparison of the ATR-FT-IR spectra of the composites prepared by varying means with the spectrum of the unfilled elastomer. [Color figure can be viewed in the online issue, which is available at wileyonlinelibrary.com.]

through different preparative means. The XRD pattern for the polymer did not undergo any significant change upon nanofiller incorporation. Moreover, amorphous nature of the silica nanofiber was also confirmed due to the absence of any additional peaks (due to the presence of nanoparticles) in the composites prepared by different means. *In situ* prepared composites showed similar XRD pattern when compared with that of the *ex situ* prepared samples. Even, higher concentration of nanofiller did not have any effect on the XRD profile of the composite. Calcined nanofibers hardly affected the nature of the XRD plot of the composites as evident from Figure 6. PDMS shows cold crystallization as observed in literature.[41] This phenomenon is evident from the DSC studies described in subsequent section. In this room temperature XRD analysis, the unfilled as well as filled PDMS vulcanizates show a characteristic broad peak around 12.5°. This might be due to some residual crystallinity (although very small) even at room temperature for PDMS.

**ATR-FT-IR Spectroscopy.** Figure 7 shows a comparison of the ATR-FT-IR spectra of the silica nanofiber/PDMS composites at the same filler content with the unfilled elastomer. Successful composite formation was evidenced by prominent shift in various peak positions of the polymer. A glance into the FT-IR spectrum shows that PDMS shows a double humped peak in the region 1090 to 1020 $cm^{-1}$ which is attributed to asymmetric Si-O-Si stretching. Besides these two, there are several other peaks corresponding to the Si-$CH_3$ functionalities around 1260 $cm^{-1}$ (due to symmetric $CH_3$ deformation) and 2900 $cm^{-1}$ (ascribed to asymmetric CH stretching).[42] It was observed that the composites irrespective of the method of preparation showed significant shift in peaks for asymmetric Si-O-Si stretching. While for unfilled elastomer the peak appeared at 1039 $cm^{-1}$, the composites showed the same peak in the range of 1012 to 1009 $cm^{-1}$. However, it is noteworthy that the peak at 1260 $cm^{-1}$ did not necessarily undergo shift in position. Hence, it is established that interaction of the polymer with the nanofiller takes place through the Si-O linkages.

According to Maiti and Bhowmick,[43] the shift in peak position toward lower wavenumber implies a negative enthalpy change and hence a thermodynamically facilitated process. A brief insight into the thermodynamics of composite formation divulges the fact that for successful composite preparation, free energy of the system is formulated as:

$$\Delta Gs = \Delta Hs - T\Delta Ss \tag{7}$$

The process of composite formation will be thermodynamically facilitated when $\Delta Gs$ is negative.

In this equation,

$$\Delta Gs = \Delta G_E + \Delta G_C = (\Delta H_E + \Delta H_C) - T(\Delta S_E + \Delta S_C) \tag{8}$$

where,

$$\Delta G_E = \Delta H_E + T\Delta S_E \quad \text{for the polymer} \tag{9}$$

$$\Delta G_C = \Delta H_C + T\Delta S_C \quad \text{for the nanofiller} \tag{10}$$

Here, the changes in enthalpy and entropy of the polymer and the nanofiller during the process of composite formation are designated by the symbols $\Delta H_E$, $\Delta H_C$, $\Delta S_E$, and $\Delta S_C$.

Quantitatively, the shift in peak position can be related to the enthalpy change of the system by using the Fowkes's equation as follows:[44]

$$\Delta H_S = 0.236 \times \Delta v \tag{11}$$

Enthalpy change was calculated for all the composite systems. It was observed that all the composites showed significantly high negative $\Delta G$ values (Table II). Although there was no significant alteration in $\Delta G$ values for the composites, the magnitude was relatively slightly higher for *in situ* prepared composites. *Ex situ* prepared composites with toluene as the solvent showed slightly lower $\Delta G$ value compared with that of the composite prepared with THF as the solvent. There was not much change in $\Delta G$ value with higher loading of nanofiller. Besides this, the sample prepared with calcined silica nanofiber showed lower $\Delta G$ value compared with the uncalcined one. An endeavor to estimate free energy change during composite preparation necessitates determination of entropy of mixing by exploring the Flory-Huggins theory as follows:[45–47]

$$\Delta Ss = -k[N_C \mathrm{In}(N_C/N) + N_E \mathrm{In}(xN_E/N)] \tag{12}$$

Or,

$$\Delta Ss = -k[N_C \mathrm{In}(\phi_C) + N_E \mathrm{In}(\phi_E)] \tag{13}$$

$$\phi_C = N_C/N \text{ and } \phi_E = xN_E/N \tag{14}$$

In the above equations, $\phi_C$ and $\phi_E$ designate the volume fractions of the silica nanofibers and polymer, respectively and the

**Table II.** Calculation of Enthalpy and Free Energy Change During Composite Formation

| Composite | Shift in peak position at 1039 $cm^{-1}$ ($\Delta\nu$) | Enthalpy change $\Delta H$ (kcal/mol) | Free energy change $\Delta G$ (kcal/mol) |
|---|---|---|---|
| VPSU2I | 33 ± 1 | −7.788 ± 0.236 | −7.789 ± 0.236 |
| VPSU2(THF) | 30 ± 1 | −7.080 ± 0.236 | −7.081 ± 0.236 |
| VPSC2(THF) | 29 ± 2 | −6.844 ± 0.472 | −6.845 ± 0.472 |
| VPSC2I | 30 ± 1 | −7.080 ± 0.236 | −7.081 ± 0.236 |
| VPSU2(TOL) | 30 ± 3 | −7.080 ± 0.708 | −7.081 ± 0.708 |

respective number of molecules are expressed as $N_C$ and $N_E$. Here, $k$ is the Boltzmann's constant.

Similar attempt was made in determining the free energy change for HA nanofiber/PDMS composite system.[48] Entropic contribution was found to be negligible in comparison with the enthalpic one. This is probably due to the fact that the entropy increase due to debundling effect of the silica nanofibers is almost nullified by the entropy loss due to penetration of polymer molecules in the aggregated nanofiller. The hydrogen bonding interaction between filler silanol groups and the polymer molecules is plausibly responsible for the enhanced enthalpic contribution to the energy change. The results are summarized in Table II.

**Differential Scanning Calorimetry Studies.** Figure 8 shows the comparison of the DSC thermograms of virgin and silica nanofiber (2 wt %) filled *in situ* prepared composite. The glass transition is observed around −125°C for the unfilled elastomer. Besides this, two other peaks are observed at around −100°C and −36°C. The former peak is assigned to the crystalline domain formation and the latter is due to melting of the crystalline domains.

It is observed that the glass transition temperature does not show any prominent change in position upon composite formation. Moreover, the melting peak is found to undergo a prominent shift towards lower temperature side with slight broadening upon silica nanofiber incorporation. This is in coherence with the observation of Fragiadakis et al.[30]

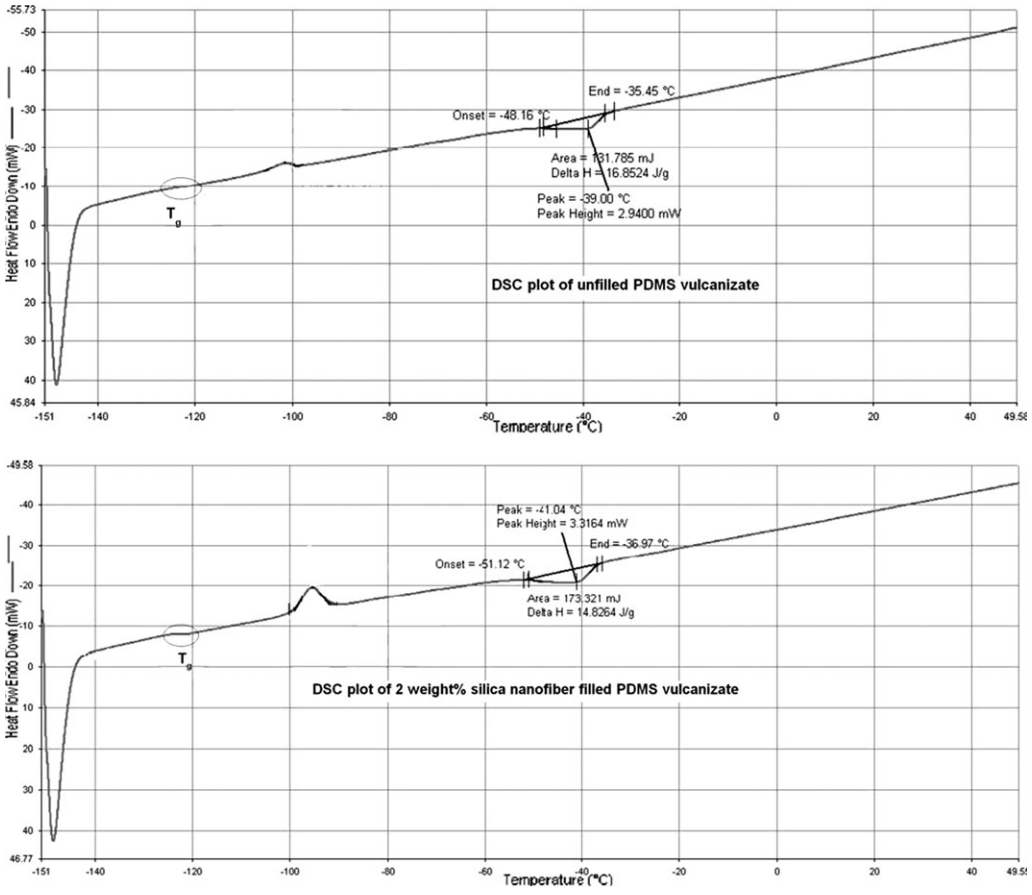


**Figure 8.** Comparison of the DSC thermograms of unfilled and filled PDMS vulcanizates.

**Table III.** Comparison of Crosslink Density of the Composites

| Nanocomposite | Crosslink density $\times 10^{-5}$ (mol/cm$^3$) |
|---|---|
| VPS0 | 1.90 |
| VPSU2(TOL) | 5.44 |
| VPSU2(THF) | 8.60 |
| VPSU2I | 8.90 |
| VPSU4I | 9.63 |
| VPSU6I | 4.82 |
| VPSU′4I | 3.00 |
| VPSU″4I | 7.60 |

**Interfacial Interaction Energy, Work of Adhesion, and Swelling Studies.** The phenomenon of composite formation can be considered as the wetting of the nanofiller surface by the polymer.[49,50] Contact angle measurements were carried out with unfilled PDMS in order to determine the surface energy of the polymer. Calculations showed that the surface energy value ($\gamma_s$) of synthesized vinyl endcapped PDMS was 22.68 mJ/m$^2$. The value of $\gamma_{s'}$ is obtained from literature.[37] The value was 151 mJ/m$^2$. Using this value, the interfacial interaction energy ($\gamma_{s's}$) for the composite formation was calculated and was found to have a value of 74.21 mJ/m$^2$. Subsequently, work of adhesion showed a value of 99.47 mJ/m$^2$. This suggested that wetting of the silica nanofiber surface by the PDMS molecules was good. In other words, it can be said that composite formation was aided by good polymer-nanofiber interface formation.

Crosslink densities of the composites were also determined through swelling studies in order to get an idea of the strength of the polymer-filler interface. The results of this study are compiled in Table III. It was observed the *in situ* prepared composites showed higher crosslink densities compared with the *ex situ* prepared composites at the same nanofiller loading. Moreover, crosslink density increased with increase in filler loading up to 4 wt % of silica nanofiber concentration. With further increase in nanofiller concentration, it decreased drastically. The consequence of the variation of crosslink densities was reflected in the properties of the composites as discussed in the subsequent sections. The reason for the increase in crosslink density was due to non-covalent interaction between the polymer and the nanofiller and hence due to strong polymer-filler interface formation.

**Properties of the Composites**

**Dynamic Mechanical Analysis.** This study reveals the influence of various silica nanofibers on the dynamic mechanical properties of PDMS, by comparing storage modulus ($E'$) of the virgin PDMS elastomer with that of the composites prepared through various means as shown in Figure 9(a). Figure 9(b) is a comparison of the tan $\delta$ versus temperature plots of the polymer and its composites with silica nanofibers. The *in situ* prepared composite showed higher room temperature storage modulus compared with that of the THF cast *ex situ* composite at 2 wt % nanofiller loading. This was evident from a momentous increase of 175% in storage modulus for the *in situ* prepared composite VPSU2I. This improvement in storage modulus was due to better dispersion of the nanofiller in the PDMS matrix when composite was prepared through *in situ* polymerization technique. From the HRTEM studies, it is evident that the *in situ* prepared composites demonstrated highest degree of dispersion with individual nanofibers properly distributed in the PDMS matrix. In the *in situ* preparative method, polymerization takes place in presence of nanofiller. This technique facilitates polymer molecules to grow in presence of the nanofiller thereby debundling them and improving the degree of dispersion.

For *ex situ* prepared composites, it was observed that improvement was better when THF was used as the solvent for composite preparation. While VPSU2(TOL) showed 19% decrease in storage modulus at 25°C, the latter increased around 10% for VPSU2(THF) (Table IV). The composites prepared with toluene showed prominent agglomerates and bundled nanofibers in the HRTEM images. The result of this poor dispersion was reflected in the decline in properties of those composites prepared with toluene as solvent. On the other hand, the composites prepared with THF showed comparatively better dispersion of the nanofiller and consequently a higher modulus (although much lower compared with the *in situ* prepared composite). Since the amount of the nanofiber remained unchanged, the difference in property-improvement was dependent on the extent of dispersion of the nanofiller in the polymer matrix. It is clear that distribution of the nanofibers was better for the *ex situ* prepared samples with THF as the solvent. This is apparent from the results in Table IV.

Storage modulus did not show any significant change upon increase in nanofiber concentration. For the *in situ* prepared composite with 4 wt % of silica nanofiller SU, modulus increased by 40% which was much lower compared with the 2 wt % nanofiller loading. With further increase in nanofiller loading, the modulus of the composite further decreased. This was probably due to significant nanofiber agglomeration at higher concentration.

The composites prepared with the calcined nanofibers showed lower improvement in storage modulus at room temperature compared with those prepared with uncalcined nanofiller. While VPSU2I showed 175% increase in $E'$, the increase was around 150% for VPSC2I. This was probably due to reduced number of effective interlocking points between the polymer and the calcined nanofiller with distinct contours. In the case of uncalcined nanofibers, the uneven nanofiller surface possibly facilitates better polymer molecule anchorage and hence polymer-nanofiller interaction. This is depicted in Figure 9(c).

Aspect ratio of the nanofiller has a prominent impact on the dynamic mechanical properties of the composites. Storage modulus of the composites prepared with SU′ and SU″ was determined. While VPSU″4I showed 118% improvement in storage modulus at 25°C, improvement was 31% for VPSU′4I. The difference in improvement was due to difference in degree of dispersion as discussed in the composite morphology section. It was observed that with increase in aspect ratio of the nanofiber, dispersion was better and property improvement was appreciable. However, with tremendous increase in aspect ratio of the

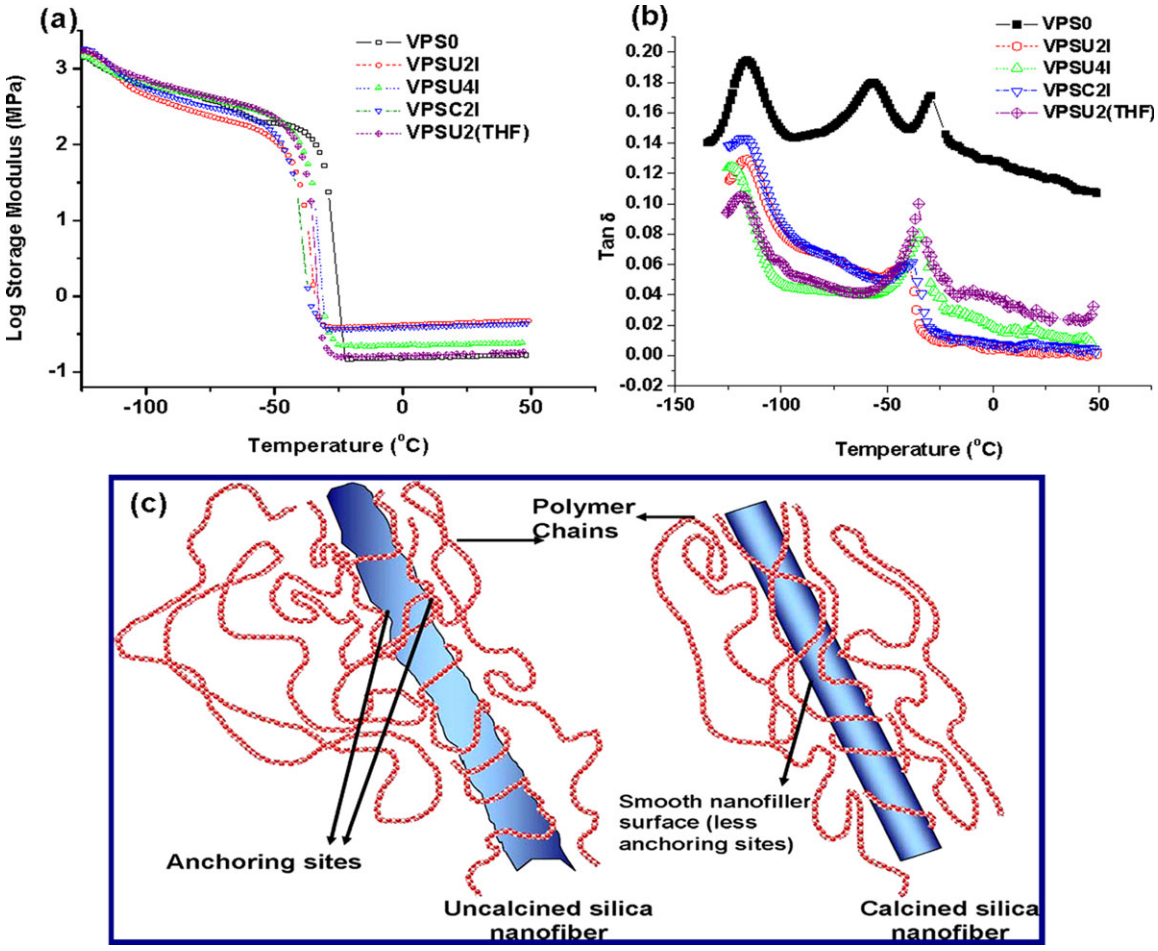


**Figure 9.** Comparison of (a) storage modulus and (b) tan $\delta$ versus temperature plots for silica nanofiber/PDMS composites prepared by various methods and (c) pictorial representation of polymer molecules anchorage on uncalcined and calcined nanofiller surface. [Color figure can be viewed in the online issue, which is available at wileyonlinelibrary.com.]

nanofiber, entanglement is a very common phenomenon as was observed with SU′ [Figure 5(h)]. Hence, in this case, proper dispersion was difficult which led to deterioration in properties.

A critical examination of the storage modulus plots divulges some interesting features. Despite the fact that the *in situ* prepared composites showed enhanced high temperature modulus compared with the *ex situ* prepared composites, low temperature modulus (in the temperature range −115 to −20°C) was much lower compared with the unfilled elastomer. For the *ex situ* prepared composites, the improvement in the low temperature modulus was only marginal. This anomaly of the low temperature behavior of PDMS is due to the presence of microcrystalline domains along with extended amorphous zones. Dimensionally though small, these crystalline domains add to the modulus of the polymer matrix. This is ascribed to the physical crosslinking nature of these microcrystallites or spherulites. The phenomenon of cold crystallization is confirmed from the DSC analysis of the unfilled and filled PDMS systems. It was observed that in presence of nanoparticulates these domains experience reduction in number and size compared with those in the virgin elastomer. The reduction in crystalline morphology of PDMS in presence of nanofiber could be correlated with the significant decrease in the low temperature storage modulus of the *in situ* prepared composites as well as the *ex situ* prepared composites. Decrease is more prominent in the case of *in situ* prepared composites due to the virtue of the preparative means.

Tan $\delta$ versus temperature plots [shown in Figure 9(b)] discloses a handful of interesting events. The presence of microcrystalline

**Table IV.** Comparison of Storage Modulus and tan $\delta$ Values for the Composites

| Sample | $E'$ at −120°C (MPa) | $E'$ at 25°C (MPa) | tan δ at $T_g$ |
|---|---|---|---|
| VPS0 | 1210 | 0.164 | 0.195 |
| VPSU2(TOL) | 2320 | 0.133 | 0.147 |
| VPSU2(THF) | 1560 | 0.180 | 0.105 |
| VPSU2I | 1440 | 0.444 | 0.130 |
| VPSU4I | 1250 | 0.230 | 0.125 |
| VPSC2I | 1650 | 0.415 | 0.144 |
| VPSU′4I | 1630 | 0.215 | 0.156 |
| VPSU″4I | 1540 | 0.357 | 0.128 |

domains in PDMS was confirmed from the appearance of peaks around −57°C and −30°C which are respectively due to formation and melting of the microcrystalline domains.[41,51] A detailed analysis of the plots revealed that while the unfilled rubber showed three prominent peaks one at glass transition temperature $T_g$ (−117°C) along with the other two mentioned earlier,[52] the peaks concerned with crystalline domains exhibited significant distortion and reduction in intensity. This was due to restriction in the microcrystalline domain formation in presence of the nanoparticles which is in coherence with the DSC studies. The attainment of the native orientation of the polymer chains was restricted by the nanoparticles when composite was prepared by any of the techniques. No shift in $T_g$ was observed confirming the fact that the nanofiller rarely affected the amorphous regions of the polymer. However, lowering of the peak height at $T_g$ was well discernible confirming the fact that polymer-filler interaction was quite obvious.

**Mechanical Properties.** Reinforcement phenomenon of various composites is comprehensible from the analysis of mechanical properties of the prepared composites. The results of this study are provided in Table IV. *In situ* prepared composites, in general, showed higher improvement in tensile strength and tensile modulus compared with the *ex situ* prepared composites. For the *in situ* prepared composite with 2 wt % silica nanofiber (VPSU2I), improvements in tensile strength and tensile modulus were 70 and 105%, respectively. This was due to better dispersion of the individual nanofibers in the polymer matrix as evident from the HRTEM micrograph in Figure 5(c).

For the *ex situ* prepared composites, samples prepared with THF as solvent showed better properties. For instance, tensile strength and tensile modulus, improvement was 23 and 40%, respectively for VPSU2(THF). Tensile strength reduced by 14% for toluene cast sample VPSU2(TOL). The difference in the property improvement or deterioration is entirely reliant to the difference in the extent of dispersion of the nanofiller in the PDMS matrix as evident from the HRTEM micrograph shown in Figure 5. For the composites prepared through solution blending technique, the extent of dispersion of the silica nanofibers is governed by the solubility parameter and interaction parameter of the polymer and the nanofiller respectively.[53] In order to get a thorough knowledge of the solubility parameter of polymer, Hoffman and van Krevelen method of additive group contribution was reviewed as follows:

$$\delta = \frac{\sum F_i}{V} = \frac{\rho \sum F_i}{M} \tag{15}$$

where $F_i$ is the contribution by the various chemical groups in the repeating unit of the polymer and the nanofiller. On the other hand, solubility parameter of silica was obtained from literature.[54]

Next, Hildebrand solubility parameter was used to calculate the interaction parameter for polymer-solvent and nanofiller-solvent systems.

For polymer-solvent pair,

$$\text{Interaction parameter } \chi_{PS} = \frac{(V_M)}{RT}(\delta_p - \delta_s)^2 \tag{16}$$

For nanofiller-solvent pair,

$$\text{Interaction parameter } \chi_{NS} = \frac{(V_M)}{RT}(\delta_N - \delta_s)^2 \tag{17}$$

where $\delta_P$, $\delta_N$, and $\delta_S$ denotes solubility parameter for the polymer, nanofiber, and solvent respectively and $V_M$, $R$, and $T$ represent molar volume of the solid (polymer/nanofiber) segment, gas constant, and temperature, respectively.

Using van Krevelen's values of cohesive energy density contribution by various groups, the $\Sigma F_i$ value for PDMS was calculated. From this $\delta_P$ was found to be 14.35 $[(\text{MPa})]^{1/2}$. In addition, literature provides a $\delta_F$ of 29.58 $[(\text{MPa})]^{1/2}$ for the nanofiber.[54] These values were used to determine the interaction $\chi_{PS}$ and $\chi_{NS}$ and hence the difference in interaction parameter was estimated. For THF cast sample, difference in interaction parameter was 1.12 which was lower compared with the toluene cast system (1.35). In line with the observation of Choudhury and Bhowmick,[53] the lesser the difference in interaction parameters $\chi_{PS}$ and $\chi_{NS}$, more is the improvement in properties. Hence, improvement was higher in the case of THF cast system.

With increase in nanofiller concentration, there was an increasing trend in the properties of the composites up to a certain critical concentration. Above this concentration, no further property enhancement was noticeable, which may be due to filler agglomeration at higher concentration. Tensile strength and tensile modulus for *in situ* prepared composites with 2, 4, and 6 wt % of silica nanofiber showed tensile modulus improvement of 145%, 250%, and 317% and tensile strength improvement of 41%, 122%, and 34% respectively. With higher nanofiber concentration, the composites did not exhibit any further improvement in mechanical properties. These increments were much higher compared with the THF cast *ex situ* sample. This was evident from the tensile strength improvement which was just 29% for *ex situ* prepared VPSU4(THF). With further increase in nanofiller concentration, property-improvement was only marginal compared with the unfilled PDMS elastomer. This minimal improvement was due to predominant nanofiller agglomeration.[55]

When nature of the nanofiller was taken into consideration, composites prepared with calcined silica nanofibers displayed lower improvement compared with uncalcined nanofiller containing composites. As observed from the results in Table V, while enhancement in tensile strength was 70% for the composite prepared with 2 wt % of uncalcined silica nanofiber (VPSU2I), it was about 60% for the composite with calcined nanofiber at same nanofiller loading (VPSC2I). The reason is same as mentioned in the dynamic mechanical analysis section.

Variation of aspect ratio has a prominent impact on the mechanical properties of the composites. For VPSU′4I, the tensile strength and tensile modulus showed minimal improvement due to very high aspect ratio of the nanofibers. On the other hand, VPSU″4I, showed better properties compared with

**Table V.** Comparison of Mechanical and Thermal Properties of the Composites

| Composite | *E* modulus (kPa) | Tensile strength (kPa) | Temperature of maximum degradation $T_{max}$ (°C) | Temperature of onset of degradation (°C) | Ash content (%) |
|---|---|---|---|---|---|
| VPS0 | 140 ± 20 | 167 ± 12 | 350 | 332 | 18.25 |
| VPSU2 (TOL) | 183 ± 12 | 143 ± 41 | 438 | 378 | 18.76 |
| VPSU2 (THF) | 196 ± 23 | 206 ± 22 | 484 | 402 | 22.02 |
| VPSU4 (THF) | 346 ± 31 | 216 ± 13 | 496 | 430 | 29.10 |
| VPSC2 (THF) | 200 ± 12 | 188 ± 17 | 461 | 407 | 24.78 |
| VPSU2I | 343 ± 9 | 236 ±6 | 533 | 446 | 33.82 |
| VPSU4I | 489 ± 32 | 371 ± 17 | 541 | 466 | 33.22 |
| VPSU6I | 584 ± 40 | 222 ± 28 | 519 | 453 | 31.06 |
| VPSC2I | 291 ± 19 | 224 ± 15 | 505 | 455 | 30.66 |
| VPSU′4I | 229 ± 9 | 184 ± 22 | 498 | 415 | 43.08 |
| VPSU″4I | 457 ± 16 | 203 ± 23 | 521 | 462 | 34.33 |

VPSU′4I since the nanofibers showed an average lower aspect ratio of 4.02 and dispersion was facilitated. Tensile strength and tensile modulus improvements were, however, lower compared with VPSU4I. Hence, an optimal aspect ratio in required for proper dispersion of the nanofibers in the polymer matrix.

**Thermal Properties of the Composites.** A comparison of the thermogravimetric traces of the composites is provided in Figure 10 in order to understand the effect of silica nanofiber in improving oxidative thermal stability of the composites. The results of the thermal analysis are shown in Table V. Thermal stability was observed to be a function of extent of nanofiller dispersion. This was reflected in the temperature of maximum degradation ($T_{max}$) and the temperature of onset of degradation ($T_i$) for the composites as well as the ash content for the composites prepared through different techniques.

*In situ* prepared composites showed highest thermal stability among all the composites. For 2 wt % silica nanofiller loaded *in situ* composite, $T_{max}$ and $T_i$ were observed to be 533 and 446°C, respectively. This is probably due to better state of dispersion of the silica nanofibers in the polymer matrix compared with other composites.

*Ex situ* composites were prepared using two different solvent systems. It was observed that composites prepared with THF as solvent showed better oxidative thermal stability compared with the toluene cast samples. While VPSU2(THF) showed $T_{max}$ of 484°C, it was 438°C for VPSU2(TOL). The obvious reason for this difference is the difference in nanofiller dispersion which, in turn, affects the interface formation or sample inhomogenity. Good nanofiber dispersion promotes stronger polymer-filler interface formation and hence restrict facile removal of the volatiles during polymer degradation.

Higher filler loading did not significantly affect the thermal stability of the composites probably due to nanofiber agglomeration. Up to 4 wt % of nanofiber, the *in situ* prepared composites showed increase in $T_{max}$ and $T_i$. However, with higher filler loading, there was no significant change. While for VPSU4I, $T_{max}$ was documented to be 541°C, it was 519°C for VPSU6I. Moreover, composites prepared with calcined nanofiber showed lower $T_{max}$ and $T_i$ values when compared with those of the composites prepared same amount of uncalcined nanofiller. For instance, $T_{max}$ for VPSU2I was 533°C, while for VPSC2I it was found to be 505°C. The probable reason might be lower polymer-filler interface formation due to well defined contour and smooth surface of the calcined nanofiller. The results of thermogravimetric analysis are recorded in Table V.

The basic mechanistic approach in thermal stability improvement is the barrier mechanism of the fibrous nanofiller present in the polymer matrix. Proper nanofiller dispersion in the PDMS matrix facilitates stronger polymer-filler interface formation. When the nanofibers are well distributed in the polymer matrix as shown in the inset of Figure 10, heat transmission takes place along tortuous paths. The stronger interface provides thermal resistance thereby enhancing thermal stability of the composites.[56] This prevents facile passage of the volatiles and decomposition products from the rubber surface and hence enhances the thermal stability. However, when nanofibers are present unevenly throughout the matrix as agglomerates, heat transmission takes place primarily through the regions where nanofillers are absent. In another way, the agglomerates formed serve as heat conducting machineries.[57] These aggregates accelerate the loss of cyclics and other degradation products. Hence, proper nanofiller dispersion is an essential criterion for upliftment of oxidative thermal stability of the composites. Furthermore, ash content was found to be non-stoichiometic and independent on the amount of the nanofiller present. It was established that the composite with higher thermal stability yielded higher ash residue and *vice versa*. This observation has coherence with those in our previous work and the reason has been explained therein.[27]

Thermal stability of the VPSU′4I and VPSU″4I was investigated and compared with that of VPSU4I. It was observed that thermal stability of VPSU″4I was more compared with that of VPSU′4I. This was probably due to nanofiber agglomeration in case of VPSU′4I due to its too high aspect ratio as mentioned earlier. Moreover, thermal stability of both these composites was lower than that of VPSU4I. Hence, an optimal aspect ratio of the nanofiber is essential for the exhibition of the barrier mechanism efficiently.

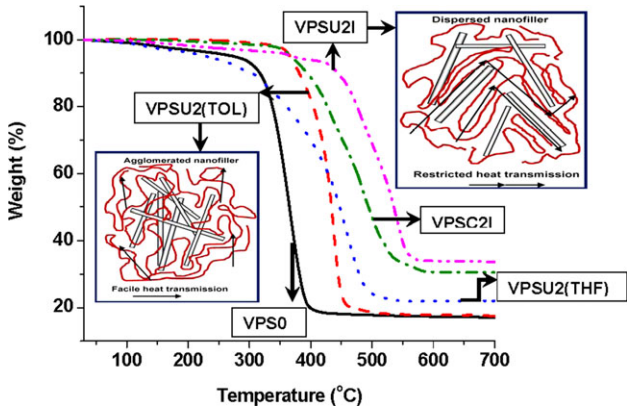


**Figure 10.** Comparison of the TGA traces of the unfilled PDMS and its composites prepared with uncalcined and calcined silica nanofibers. [Color figure can be viewed in the online issue, which is available at wileyonlinelibrary.com.]

## CONCLUSIONS

This work is a compilation of the synthesis of silica nanofibers using surfactant mediated template process. The nanofibers synthesized were characterized in terms of morphology through HRTEM, and chemical structure using FT-IR spectroscopy. Crystallinity of the nanofibers was determined using WAXD analysis while surface area of the nanofiller was estimated through BET $N_2$ adsorption studies. The nanofibers were found to possess fiber like structure with mean diameter of 80 nm for uncalcined nanofibers and 60 nm for calcined nanofibers and length ranging between few micrometers. The presence of Si-O-Si and Si-OH linkages was confirmed from FT-IR spectroscopy analysis. However, the material in the uncalcined as well as calcined form exhibited no diffraction peak in the XRD analysis suggesting complete amorphicity. BET analysis provided a surface area value of 222 $m^2$/gm. Silica nanofiber was also synthesized by varying the amount of the surfactant. It was found that with increase in amount of the surfactant, the aspect ratio of the nanofiber reduced.

Our main aim in this study was the successful synthesis of the composite using this novel nanoparticle. Composites were prepared through *in situ* polymerization and conventional solution mixing techniques. All the preparation techniques proved effective for the composite synthesis. The facile nature of composite formation was determined from the negative free energy value for the system. The *in situ* prepared composite showed highest magnitude of negative free energy. The difference in the free energy value was probably dependent on the extent of nanofiber dispersion in the PDMS matrix. This was determined through HRTEM studies. The outcome of difference in nanofiber dispersion was reflected in the various property improvements. Composite preparation, however, restricted the phenomenon of low temperature crystallization of PDMS. This was determined through DSC studies. The *in situ* prepared composites showed maximum improvement in mechanical, dynamic mechanical and thermal properties. Storage modulus improvement of the VPSU2I was 175% at 25°C while for VPSU2(THF) improvement was only 45%. Tensile modulus improved by 105% and 40% respectively for VPSU2I and VPSU2(THF). For the solution cast composites, the one with better distribution (THF as processing solvent) gave more improvement in properties. The *in situ* prepared composites showed highest thermal stability among all the composites. For VPSU2I, $T_{max}$ was recorded to be 533°C while it was only 350°C for the unfilled one. Apart from the nanofiber dispersion factors like nanofiber calcination, restricted microcrystalline domain formation in the presence of nanofiber etc. owe their contribution in influencing the property improvement. Composite prepared with SU′ (VPSU′4I) showed inferior properties due to poor dispersion of the nanofiller in the PDMS matrix. Difficulty in the achievement of proper dispersion was due to extremely large nanofiber aspect ratio. On the other hand, VPSU″4I instead of showing good dispersion showed slightly lower properties compared with VPSU4I due to lower aspect ratio of the nanofiller. Hence, along with proper dispersion of the nanofiller in the polymer matrix, nanofiber aspect ratio is an important factor in property enhancement of the composites.

## ACKNOWLEDGMENTS

The authors are thankful to Council of Scientific and Industrial Research (CSIR), New Delhi, India, for the financial assistance provided for pursuing the work.

## REFERENCES

1. Wang, W.; Ciselli, P.; Kuznetsov, E.; Peijs, T.; Barber, A. H. *Philos. Trans. R Soc. London Ser. A* **2008**, *366*, 1613.
2. Bhattacharyyaa, S.; Sinturela, C.; Bahloula, O.; Saboungia, M.-L.; Thomas, S.; Salvetat, J.-P. *Carbon* **2008**, *46*, 1037.
3. Kojima, Y.; Usuki, A.; Kawasumi, M.; Okada, A.; Fukushima, Y.; Karauchi, T.; Kamigaito, O. *J. Mater. Res.* **1993**, *8*, 1185.
4. Yan, W.; Han, Z. J.; Phung, B. T.; Ostrikov, K. K. *ACS Appl. Mater. Interfaces* **2012**, *4*, 2637.
5. Murakami, K.; Iio, S.; Ikeda, Y.; Ito, H.; Tosaka, M.; Kohjiya, S. *J. Mater. Sci.* **2003**, *38*, 1447.
6. Dewimille, L.; Bresson, B.; Bokobza, L. *Polymer* **2005**, *46*, 4135.
7. Joly, S.; Garnaud, G.; Ollitrault, R.; Bokobza, L.; Mark, J. E. *Chem. Mater.* **2002**, *14*, 4202.
8. Arroyo, M.; Lopez-Manchado, M. A.; Herrero, B. *Polymer* **2003**, *44*, 2447.
9. Valadares, L. F.; Leite, C. A. P.; Galembeck, F. *Polymer* **2006**, *47*, 672.
10. Lopez-Manchado, M. A.; Herrero, B.; Arroyo, M. *Polym. Int.* **2003**, *52*, 1070.
11. Samir, M. A. S. A.; Alloin, F.; Dufresne, A. *Biomacromolecules* **2005**, *6*, 612.
12. Favier, V.; Cavaillé, J.; Canova, G.; Shrivastava, S. *Polym. Eng. Sci.* **1997**, *37*, 1732.
13. Ljungberg, N.; Bonini, C.; Bortolussi, F.; Boisson, C.; Heux, L.; Cavaille, J. Y. *Biomacromolecules* **2005**, *6*, 2732.

14. Jung, Y. J.; Kar, S.; Talapatra, S.; Soldano, C.; Viswanathan, G.; Li, X.; Yao, Z.; Ou, F. S.; Avadhanula, A.; Vajtai, R.; Curran, S.; Nalamasu, O.; Ajayan, P. M. *Nano Lett.* **2006**, *6*, 413.
15. Wu, C.-L.; Lin, H.-C.; Hsu, J -S.; Yip, M.-C.; Fang, W. *Thin Solid Films* **2009**, *517*, 4895.
16. Ci, L.; Suhr, J.; Pushparaj, V.; Zhangand X.; Ajayan, P. M. *Nano Lett.* **2008**, *8*, 2762.
17. Hu, C.; Liu, C.; Zhang, Y.; Chen, L.; Fan, S. *ACS Appl. Mater. Interfaces* **2010**, *2*, 2719.
18. Roy, N.; Bhowmick, A. K. *J. Mater. Sci.* **2012**, *47*, 272.
19. Roy, N.; Bhowmick, A. K. *J. Appl. Polym. Sci.* **2012**, *123*, 3675.
20. Verdejo, R.; Barroso-Bujans, F. M.; Rodriguez-Perez, A.; de Saja, J. A.; Lopez-Manchado, M. A. *J. Mater. Chem.* **2008**, *18*, 2221.
21. Guimont, A.; Beyou, E.; Martin, G.; Sonntag, P.; Cassagnau, P. *Macromolecules* **2011**, *44*, 3893.
22. Schmidt, D. F.; Giannelis, E. P. *Chem. Mater.* **2010**, *22*, 167.
23. Roy, N.; Bhowmick, A. K. *Polymer* **2010**, *51*, 5172.
24. Alexandre, M.; Dubois, P. *Mater. Sci. Eng. R* **2000**, *28*, 1.
25. Alonso, B.; Sanchez, C. *J. Mater. Chem.* **2000**, *10*, 377.
26. Guermeur, C.; Lambard, J.; Gerard, J. -F.; Sanchez, C. *J. Mater. Chem.* **1999**, *9*, 769.
27. Roy, N.; Bhowmick, A. K. *Rubber Chem. Technol.* **2012**, *85*, 92.
28. Inagi, S.; Ogoshi, T.; Miyake, J.; Bertolucci, M.; Fujiwara, T.; Galli, G.; Chiellini, E.; Chujo, Y.; Wynne, K. J. *Chem. Mater.* **2007**, *19*, 2141.
29. Green, D. L.; Mewis, J. *Langmuir* **2006**, *22*, 9546.
30. Fragiadakis, D.; Pissisa, P.; Bokobza, L. *Polymer* **2005**, *46*, 6001.
31. Fragiadakis, D.; Pissis, P. *J. Non-Cryst. Solids* **2007**, *353*, 4344.
32. Winberg, P.; Eldrup, M.; Maurer, F. H. J. *Polymer* **2004**, *45*, 8253.
33. Aranguren, M. *Polymer* **1998**, *39*, 4897.
34. Adachi, M.; Harada, T.; Harada, M. *Langmuir* **2000**, *16*, 2376.
35. Shen, G.; Bando, Y.; Golberg, D. *J. Phys. Chem. B* **2006**, *110*, 23170.
36. Sen Majumder, P.; Bhowmick, A. K. *Radiat. Phys. Chem.* **1998**, *53*, 63.
37. Kessaissia, Z.; Papirer, E.; Donnet, J. -B. *J. Colloid Interface Sci.* **1981**, *82*, 526.
38. Bhowmick, A. K.; Hall, M. A.; Benarey, H. A. Rubber Products Manufacturing Technology; Marcel Dekker: New York, **1994**; p 317.
39. Flory, P. J.; Rehner, J. H. *J. Chem. Phys.* **1943**, *11*, 521.
40. Imae, T.; Kamiya, R.; Ikeda, S. *J. Colloid Interface Sci.* **1985**, *108*, 215.
41. Clarson, S. J.; Dodgson, K.; Semlyen, J. A. *Polymer* **1985**, *26*, 930.
42. Socrates, G. Infrared Characteristic Group Frequencies; John Wiley and Sons: Bristol, **1980**.
43. Maiti, M.; Bhowmick, A. K. *Compos. Sci. Technol.* **2008**, *68*, 1.
44. Fowkes, F. M.; Tischler, D. O.; Wolfe, J. A.; Lannigan, L. A.; Ademu-John, C. M.; Halliwell, M. J. *J. Polym. Sci. Part A: Polym. Chem.* **1984**, *22*, 547.
45. Flory, P. J. *J. Chem. Phys.* **1942**, *10*, 51.
46. Flory, P. J. *J. Chem. Phys.* **1941**, *9*, 660.
47. Huggins, M. L. *J. Chem. Phys.* **1941**, *9*, 440.
48. Roy, N.; Bhowmick, A. K. *J. Phys. Chem. C* **2012**, *116*, 8763.
49. Maiti, M.; Bhowmick, A. K. *J. Polym. Sci. Part B: Polym. Phys.* **2006**, *44*, 162.
50. Bhattacharya, M.; Maiti, M.; Bhowmick, A. K. *Polym. Eng. Sci.* **2009**, *49*, 81.
51. Burnside, S. D.; Giannelis, E. P. *J. Polym. Sci. Part B: Polym. Phys.* **2000**, *38*, 1595.
52. Alexandru, M.; Cristea, M.; Cazacu, M.; Ioanid, A.; Simionescu, B. C. *Polym. Compos.* **2009**, *30*, 751.
53. Choudhury, A.; Bhowmick, A. K. *Polymer* **2009**, *50*, 201.
54. Lafaurie, A.; Azema, N.; Ferry, L.; Lopez-Cuesta, J. -M. *Powder Technol.* **2009**, *192*, 92.
55. Yoonessi, M.; Gaier, J. R. *ACS Nano* **2010**, *4*, 7211.
56. Morimune, S.; Kotera, M.; Nishino, T.; Goto, K.; Hata, K. *Macromolecules* **2011**, *44*, 4415.
57. Yu, C.; Kim, Y. S.; Kim, D.; Grunlan, J. C. *Nano Lett.* **2008**, *8*, 4428.